PHYSICAL REVIEW C VOLUME 33, NUMBER 3 MARCH 1986

Inelastic scattering of 65-MeV polarized protons from ^{178}Hf, ^{180}Hf, ^{182}W, and ^{184}W and multipole moments of the optical potential

H. Ogawa,* H. Sakaguchi, M. Nakamura, T. Noro,† H. Sakamoto,‡ T. Ichihara,§ M. Yosoi,
M. Ieiri, N. Isshiki,** Y. Takeuchi, and S. Kobayashi
Department of Physics, Kyoto University, Kyoto 606, Japan

(Received 26 August 1985)

Differential cross sections and analyzing powers of polarized proton elastic and inelastic scattering from ^{178}Hf, ^{180}Hf, ^{182}W, and ^{184}W have been measured at 65 MeV. Analysis has been performed in the framework of the coupled channel formalism of the deformed optical potential for $J^{\pi}=0^{+}-6^{+}$ members of the ground state rotational band. In this analysis, all the deformation parameters of the real central, volume imaginary, surface imaginary, and spin-orbit parts of the deformed optical potential were searched independently. Up to the 6^{+} state, excellent fits have been obtained. It is found that the quadrupole moment of the real central part is 6–9 % larger than that of the charge density for all the measured nuclei, but the quadrupole moment of the Woods-Saxon form factor of the spin-orbit part agrees with the charge quadrupole moment within the fitting error. These results are consistent with the difference between the effects of the density dependence of the effective nucleon-nucleon interaction on the real central part and the spin-orbit part of the optical potential. Similar trends are also found for the hexadecapole moments of the real central part and the spin-orbit part. A folding model calculation using a realistic effective interaction has been carried out and its results are compared to those of the coupled channel analysis.

I. INTRODUCTION

Systematic measurements of proton elastic scattering[1–5] and the progress in nuclear matter theory have brought about renewed interest in the optical potential. Recently, the subject of these studies has been extended to permanently deformed nuclei.[6–11] In this case, in addition to the volume integral and the mean square radius of the optical potential, multipole moments of the deformed nuclear potential provide new physical quantities to examine the microscopic description of the optical potential more critically. Experimentally, it is necessary to obtain the spectrum with well-separated peaks of each member of the ground state rotational band. Progress in high intensity and high quality polarized beams and high resolution spectrographs has made it possible to perform such a measurement efficiently.

One of the most interesting problems in the study of the inelastic scattering from the ground state rotational band is what relation lies among the multipole moments of the charge density, matter distribution, and the deformed optical potential (DOP). Up to now, much effort has been devoted towards solving this problem. Elastic and inelastic scattering using hadron probes[6–16] has been measured and the relation between the multipole moments of the DOP and those of the charge density[17–24] has been discussed. The polarized proton scattering is the simplest and the most productive of various hadron probes for the microscopic treatment of the optical potential because one can obtain the information on spin observables easily and needs not consider the internal structure of the projectile.

According to Satchler's theorem,[25,26] the multipole moments of the DOP should be equal to those of the matter distribution, if the DOP is derived from a folding prescription assuming that proton and neutron distributions are the same and the effective interaction is local and density independent. In our previous paper,[10] we carried out the coupled channel analysis for our experimental data of Er and Yb isotopes under the condition that each part of the DOP produced equal multipole moments. As the result of this analysis, it was found that the quadrupole moments of the DOP are 4–6 % larger than those of the charge density and that these differences are mainly attributed to the density dependence of the effective interaction.

We have measured the cross sections and the analyzing powers of polarized proton elastic and inelastic scattering from ^{178}Hf, ^{180}Hf, ^{182}W, and ^{184}W at 65 MeV as an extension of our systematic measurements of elastic scattering[1] and inelastic scattering from rare earth nuclei.[9,10] In our previous paper, the coupled channel analysis was performed under the condition that each part of the DOP produced equal multipole moments. The fitting to the experimental data for the 6^{+} state was not so good as for the lower excited states. In the present work, we have measured the 6^{+} state with much higher statistics and carried out another coupled channel analysis to fit the data up to the 6^{+} state without the above condition. In addition, we have investigated the relations among the multipole of the real central, imaginary, and spin-orbit parts of the DOP.

The experimental data using 65 MeV polarized protons are thought to be valuable because of the simplicity of the reaction mechanism; they are relatively free from the giant resonance effects and the multistep processes observed in the lower energy region. Furthermore, in this energy region the real central part of the optical potential is deep, in contrast to the intermediate and high energy region,

©1986 The American Physical Society

where the imaginary part of the optical potential plays an important role. In addition, the DOP parameters can be determined with fewer ambiguities by using the analyzing power data together with the cross sections. In Sec. II, the experimental procedure and the method of the data reduction are summarized. The coupled channel analysis and its results are presented in Sec. III. The comparison of the multipole moments of the DOP derived from our experimental data with those of the charge density and with the results of the folding model calculation are given in Sec. IV. A summary and some conclusions are given in Sec. V.

II. EXPERIMENTAL METHOD

The experiment has been performed with 65 MeV polarized protons from the cyclotron at the Research Center for Nuclear Physics, Osaka University, and the data have been obtained using the high resolution spectrograph RAIDEN.[27] The details of the beam transport system were presented in our previous paper.[10]

The direction of the beam polarization was reversed every 0.5 sec by switching the rf transition at the atomic beam-type polarized ion source.[28] During the experiment the beam polarization was monitored by a sampling-type polarimeter.[29] The typical beam polarization was about 80% for both spin-up and spin-down modes and the beam intensity was 50—100 nA.

The self-supported targets used were prepared by means of the heavy ion sputtering after the deoxidization of the enriched hafnium (tungsten) oxide powder. The oxide powder was mixed with aluminum powder and deoxidized by means of the radio heating. After deoxidization, the mixed powder was preserved in hydrochloric acid for a couple of days in order to remove the aluminum oxide and the remainder of aluminum. Thus the pure hafnium (tungsten) metal powder was obtained. The details of the heavy ion sputtering are described elsewhere.[30] In the present case, 10 keV Ar ions bombarded this pure tungsten metal powder. For the hafnium powder, Kr ions were employed in order to raise the sputtering yield. The thickness and the isotope enrichment of the target foils used are listed in Table I.

The solid angles and angular acceptances were 1.3 msr and ±0.46° for measurements at forward angles ($\theta_{\text{lab}} \leq 36°$) and 2.5 msr and ±0.71° at backward angles ($\theta_{\text{lab}} > 36°$), respectively. The angular distributions were measured from 11° to about 75° in 1.0° steps at the forward angles and in 2.0° steps at the backward angles. At very forward angles ($\theta_{\text{lab}} \leq 15°$), the width of the slits in the beam transport system was adjusted in order to keep a proper counting rate (< 800 counts/sec). Also at the forward angles, in order to measure the inelastic scattering from the 4^+ and 6^+ states more efficiently, separate measurements were carried out, where the elastically scattered protons were stopped by slits placed in front of the focal plane counter system.

The scattered protons were detected by a counter array consisting of a two-dimensional position-sensitive proportional chamber of 1.5 m length, a pair of single-wire proportional chambers, and a plastic scintillation counter.[31] An event signal was generated by an energy signal from the plastic scintillator. When an event occurred, all signals from the counter array were digitized by analog-to-digital converters (ADC's) and transferred to a PDP-

TABLE I. Thickness and isotope enrichment of the target foils.

Target	Thickness (mg/cm^2)	Enrichment (%)
^{178}Hf	1.88	91.94
^{180}Hf	1.86	93.65
^{182}W	1.57[a] 3.43[b]	94.4
^{184}W	1.93	94.8

[a] This foil was used for the measurements at forward angles ($\theta_{\text{lab}} \leq 36°$).

[b] This foil was used for the measurements at backward angles ($\theta_{\text{lab}} > 36°$).

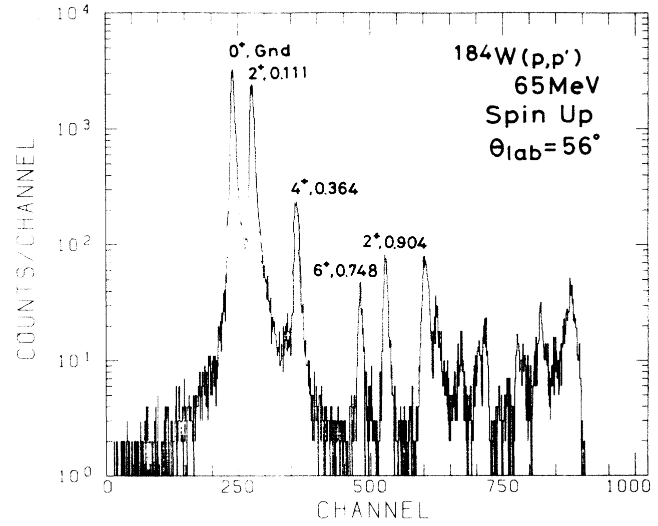

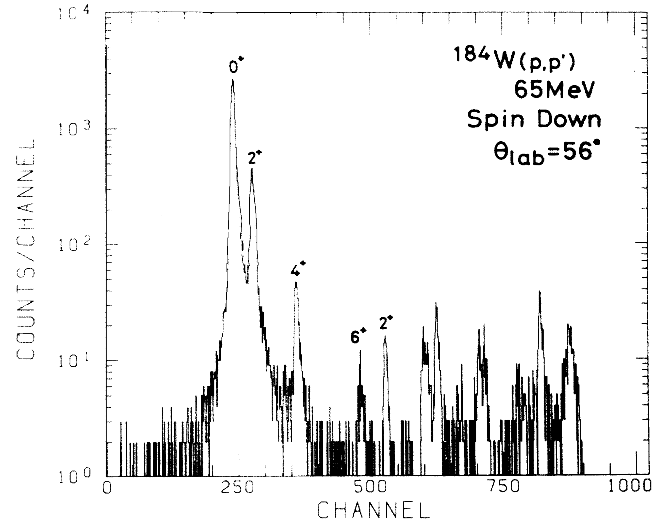

FIG. 1. Typical position spectra of the focal plane counter for the ^{184}W(p,p') scattering at 65 MeV. Spin-up and spin-down spectra are shown at $\theta_{\text{lab}} = 56°$. The states of interest to this study are labeled by their spins and parities, J^π, and excitation energies in units of MeV.

11/44 computer through the raw data processor.[32] All data were recorded on magnetic tape in a list mode.

By selecting the events which have a complete set of the signals from the counter array, the position spectra were reconstructed from the list mode raw data. The overall dead time corrections were carried out for the position spectra and these did not exceed 5%. Typical position spectra for the ^{184}W target are presented in Fig. 1. In the case of the ^{178}Hf target, the overall energy resolution was 17–20 keV FWHM at the forward angles and 23–26 keV FWHM at the backward angles. The peak areas for the 0^+, 2^+, and 4^+ states were extracted by using a peak shape fitting code.[33] The beam polarization was calculated for the spin-up and spin-down modes independently for every run. The experimental cross sections and analyzing powers are plotted in Figs. 2(a)–(d). The error bars on the experimental data represent only statistical ones.

III. ANALYSIS AND RESULTS

In the analysis of the coupled channel calculation, in order to include unknown systematic errors and to avoid trapping in an unphysical local χ^2 minimum, the errors of the cross sections and the analyzing powers were taken as follows:

$$\delta\left[\frac{d\sigma}{d\Omega}\right]=\max\left[0.03\left[\frac{d\sigma}{d\Omega}\right],\left[\frac{d\sigma}{d\Omega}\right]_{\text{statistical}}\right] \tag{1}$$

and

$$\delta A(\theta)=\max[0.03, A(\theta)_{\text{statistical}}] \; . \tag{2}$$

The renormalization factor for the experimental cross sections was also adjusted to account for the uncertainties and the inhomogenities of the target foil thickness.

Coupled channel analysis has been performed for the $J^\pi=0^+-6^+$ states of the ground state rotational band using the automatic search code ECIS79 of Raynal.[34] It was assumed that these states are members of a $K^\pi=0^+$ rotational band of the axially symmetric rigid rotor. In this analysis, the following optical potential was used:

$$\begin{aligned}U(r)={}&V_{\text{Coul}}(r)-V_R f(r;r_R,a_R)\\&-iW_v f(r;r_{wv},a_{wv})+4ia_{ws}W_s\frac{d}{dr}f(r;r_{ws},a_{ws})\\&+V_{ls}\left[\frac{\hbar}{m_\pi c}\right]^2\frac{1}{r}\frac{d}{dr}f(r;r_{ls},a_{ls})(\sigma\cdot\mathbf{L}) \; ,\end{aligned} \tag{3}$$

where

$$f(r;r_j,a_j)=[1+\exp(r-r_jA^{1/3})/a_j]^{-1} \; .$$

For the deformed optical potential, the radial parameters r_j were replaced by the angle dependent ones as

$$r_j(\theta)=r_0^j\left[1.0+\sum_\lambda \beta_\lambda^j Y_{\lambda 0}(\theta)\right] \; , \tag{4}$$

where the suffix j represents each part of the optical potential; the real central part, the volume imaginary part, the surface imaginary part, or the spin-orbit part. The deformation parameters β_2^j, β_4^j, and β_6^j were used. The full-Thomas term was used for the spin-orbit part.[35] The Coulomb potential was calculated from the deformed Fermi-type charge distribution and the reduced radius r_c and the diffuseness a_c were kept as $r_c=1.11$ fm and $a_c=0.58$ fm.[10] The DOP was expanded up to $\lambda=12$. The optical potentials and the deformation parameters were adjusted to optimize the fits to the angular distributions of the cross sections and the analyzing powers of the 0^+, 2^+, 4^+, and 6^+ states.

As discussed in our previous paper,[10] there is a problem of how to relate the deformation parameters of each part of the DOP in the coupled channel calculation. At the first stage, we have performed a coupled channel analysis on the condition that each part of the DOP produced the same value of the multipole moment of the same order (analysis 1), namely

$$\begin{aligned}Q_\lambda^R(\text{WSFF})&=Q_\lambda^{wv}(\text{WSFF})=Q_\lambda^{ws}(\text{WSFF})\\&=Q_\lambda^{ls}(\text{WSFF})=Q_\lambda^{\text{Coul}}\\&\qquad(\lambda=2,4,6) \; ,\end{aligned} \tag{5}$$

Q_λ^j(WSFF) is the Woods-Saxon form factor (WSFF) multipole moment and defined by

$$Q_\lambda^j(\text{WSFF})=\frac{Ze\int f[r;r_j(\theta),a_j]Y_{\lambda 0}(\theta)r^{\lambda+2}dr\,d\Omega}{\int f[r;r_j(\theta),a_j]r^2dr\,d\Omega} \; , \tag{6}$$

where $f[r,r_j(\theta),a_j]$ represents the WSFF of each part of the DOP given in Eqs. (3) and (4). Q_λ^{Coul} is the multiple moment of the Coulomb potential. For the real central and volume imaginary parts, the WSFF multipole moment is equal to the multipole moment of the potential itself, but not for the surface imaginary part or the spin-orbit part.

In this calculation, we have used the "modified ECIS79" which was developed in our previous work.[10] This code calculated the multipole moments of the real central part first, and then the deformation parameters of the other parts were calculated so as to reproduce the same values as those of the multipole moments of the real central part. Analysis 1 can reproduce very well the experimental results for the 0^+, 2^+, and 4^+ states. The agreement for the 6^+ state was good but not as good as for the lower excited states for the measured nuclei.

The above condition that each part of the DOP produces equal multipole moments seems to be more plausible compared with using the same deformation parameters or the same deformation length (βR). But the application of the simple folding prescription, which gives us a close relation between the matter distribution and the real central part of the optical potential, is not so straightforward for the imaginary and spin-orbit parts. Therefore we must examine the relation between the multipole moments of the same order from each part of the DOP from an experimental point of view, without any presumption. Thus we have performed another coupled channel

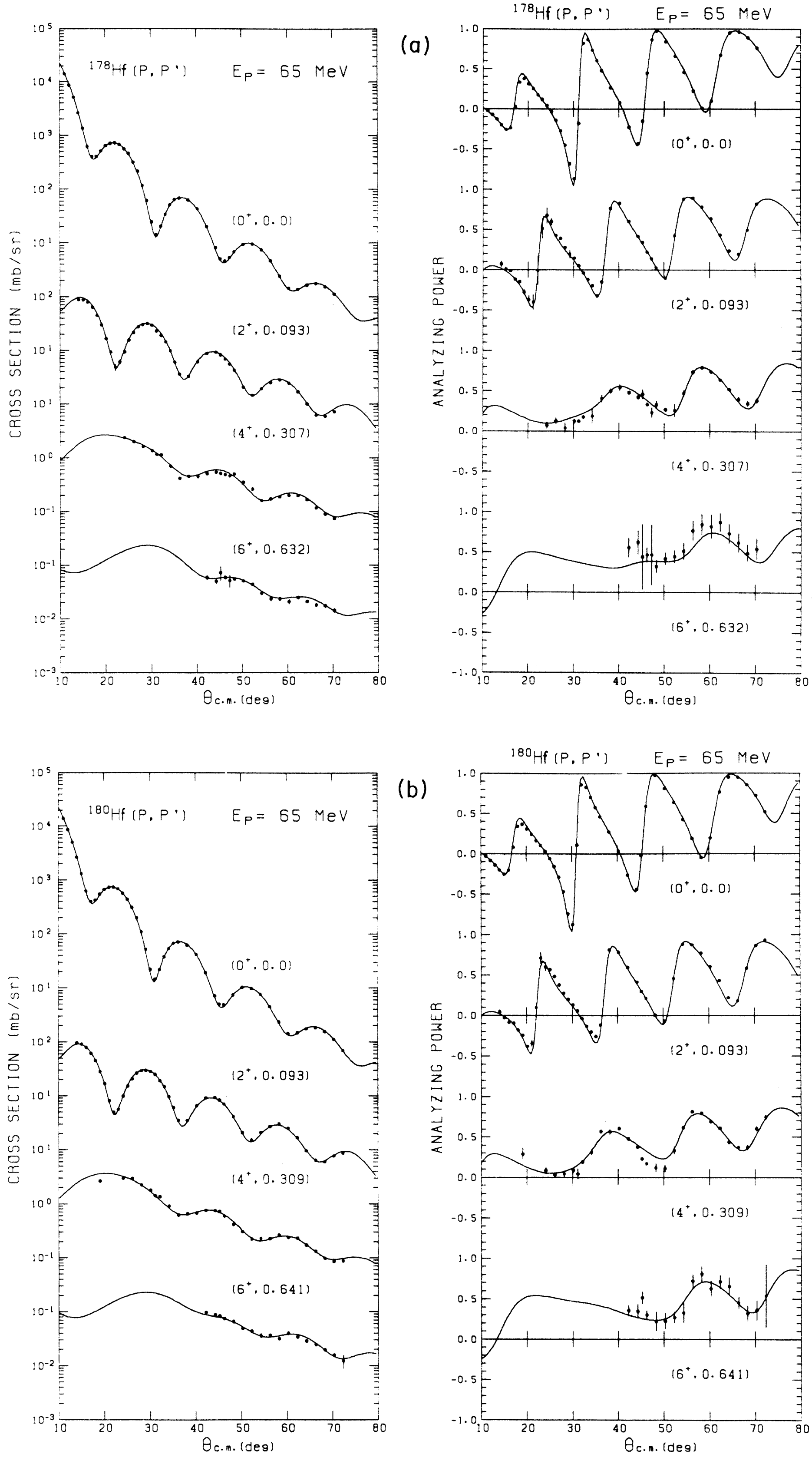

FIG. 2. (a) Measured cross sections and analyzing powers for the ^{178}Hf(p,p') scattering at 65 MeV. The solid curves represent the best fit calculations by analysis 2. (b) As for (a) except for ^{180}Hf. (c) As for (a) except for ^{182}W. As for (a) except for ^{184}W.

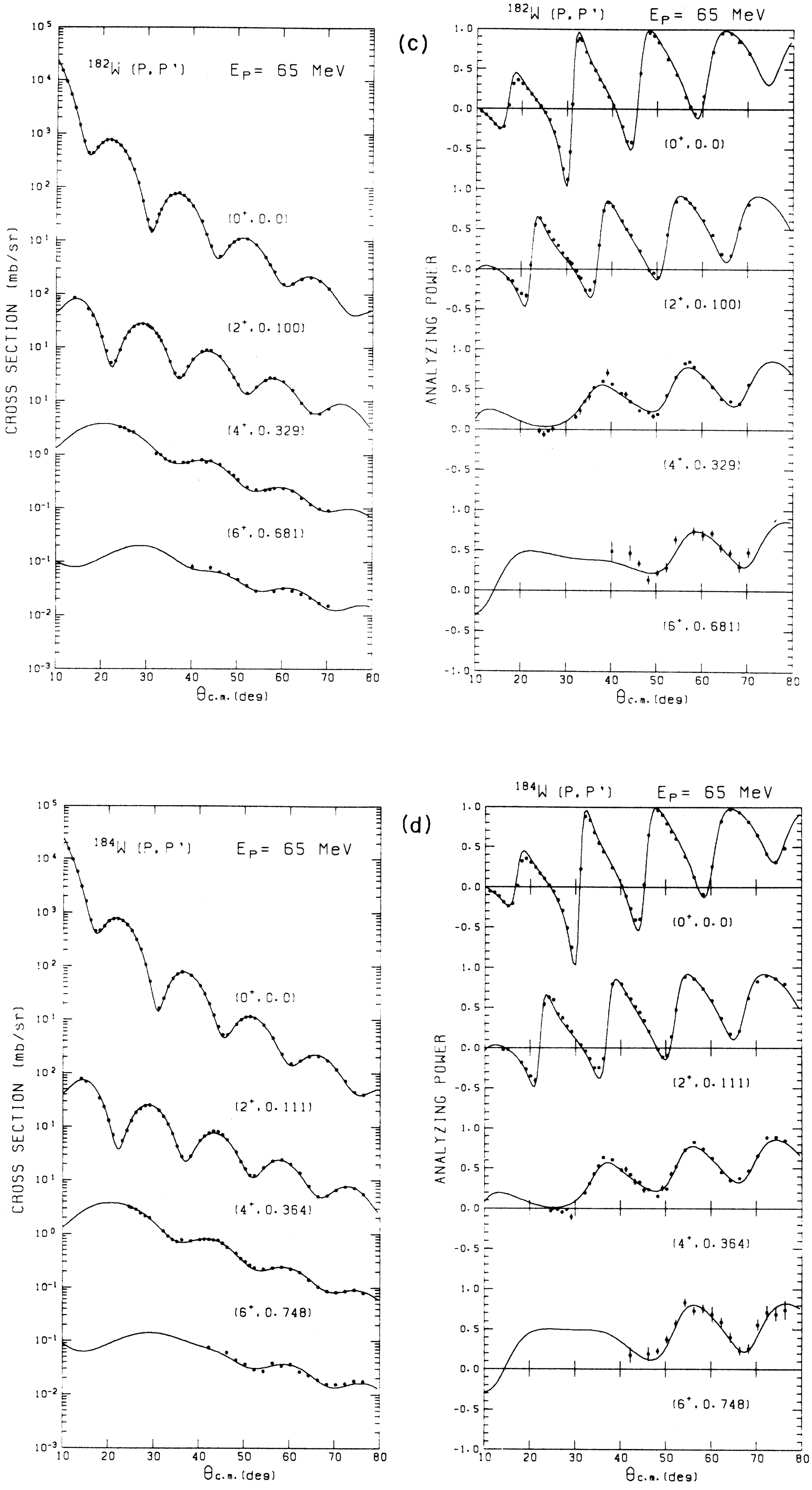

FIG. 2. (*Continued*).

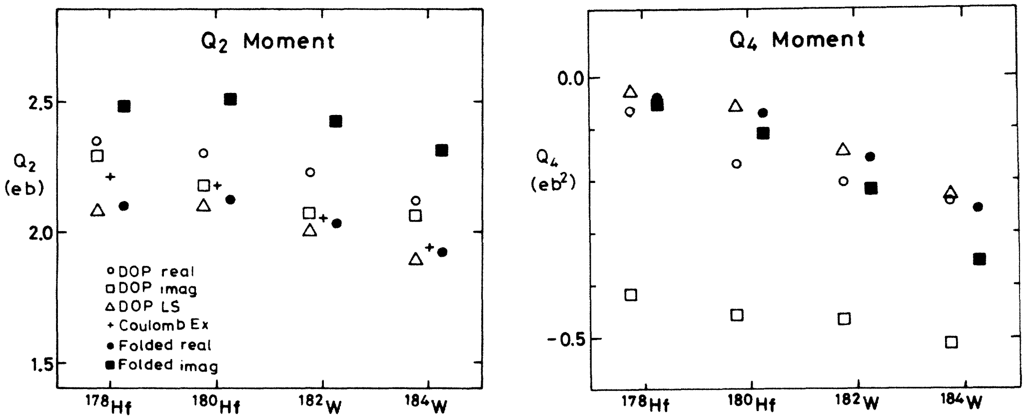

FIG. 3. The open circles and open triangles represent the WSFF multipole moments of the real central and spin-orbit parts obtained by analysis 2, respectively. The open squares represent the potential multipole moments of the imaginary part by analysis 2. The closed circles and closed squares represent the mulipole moments of the real and imaginary folded potential, respectively. The crosses represent the charge quadrupole moments obtained by the Coulomb excitation (Refs. 20 and 21).

analysis, where all the deformation parameters of each part of the DOP, except for the Coulomb potential, have been searched independently (analysis 2). Since the fitting to the experimental data was not so sensitive to the variation of the deformation parameters of the Coulomb potential, these parameters were determined so as to reproduce the same values of the multipole moments as those of the WSFF multipole moments of the spin-orbit part, namely

$$Q_\lambda^{\mathrm{Coul}} = Q_\lambda^{ls}(\mathrm{WSFF}), \quad (\lambda=2,4,6) \ . \tag{7}$$

The reason for this choice will be described in Sec. IV. The solid curves in Fig. 2 represent the results of this calculation and the DOP parameters obtained by analysis 2 are listed in Tables II and III together with the results of analysis 1. By analysis 2, the fit for the 6^+ state has been remarkably improved and also better fits than analysis 1 have been obtained for the 0^+, 2^+, and 4^+ states for all the measured nuclei.

In Fig. 3, we show the WSFF multipole moments of the real central and spin-orbit parts and the potential multipole moments of the imaginary part obtained by analysis 2 and their numerical values are tabulated in Table IV. The potential multipole moment of the imaginary part is calculated as follows,

$$Q_\lambda^w = \frac{Ze \int \left\{ W_v f[r;r_{wv}(\theta),a_{wv}] - 4a_{ws} w_s \frac{d}{dr} f[r;r_{ws}(\theta),a_{ws}] \right\} Y_{\lambda 0}(\theta) r^{\lambda+2} dr\, d\Omega}{\int \left\{ W_v f[r;r_{wv}(\theta),a_{wv}] - 4a_{ws} w_s \frac{d}{dr} f[r;r_{ws}(\theta),a_{ws}] \right\} r^2 dr\, d\Omega} \ . \tag{8}$$

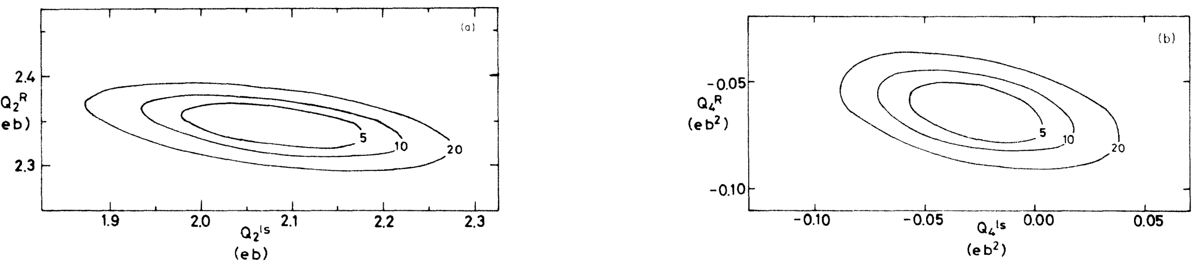

FIG. 4. (a) χ^2 contour as a function of the WSFF Q_2 moments of the real central and spin-orbit parts derived from analysis 2. (b) χ^2 contour as a function of the WSFF Q_4 moments of the real central and spin-orbit parts derived from analysis 2.

TABLE II. Best fit optical potential parameters of analysis 1 and analysis 2.

Nucleus	V_R (MeV)	r_R (fm)	a_R (fm)	W_v (MeV)	r_{wv} (fm)	a_{wv} (fm)	W_s (MeV)	r_{ws} (fm)	a_{ws} (fm)	V_{ls} (MeV)	r_{ls} (fm)	a_{ls} (fm)	$\chi^2/N(0^+)$[c]	Renorm. factor
^{178}Hf[a]	38.323	1.220	0.7284	8.087	1.093	0.8180	5.680	1.237	0.6337	5.544	1.154	0.6705	1.51	0.96
^{180}Hf[a]	37.980	1.219	0.7261	9.130	1.063	0.8043	5.417	1.252	0.6347	5.509	1.124	0.7030	1.64	0.86
^{182}W[a]	37.604	1.231	0.6976	10.075	0.869	1.0324	6.555	1.212	0.6515	5.416	1.140	0.6963	1.92	0.79
^{184}W[a]	38.439	1.217	0.7253	8.521	1.049	0.7781	5.875	1.236	0.6633	5.569	1.125	0.7110	1.67	1.19
^{178}Hf[b]	39.459	1.209	0.7159	8.590	1.345	0.6122	2.591	1.252	0.4466	5.830	1.143	0.6317	0.74	1.01
^{180}Hf[b]	39.458	1.207	0.7393	8.805	1.349	0.6203	2.040	1.259	0.4498	5.804	1.134	0.6612	0.80	0.91
^{182}W[b]	39.995	1.202	0.7424	8.290	1.259	0.5719	2.105	1.256	0.4663	5.853	1.130	0.6617	0.70	0.88
^{184}W[b]	38.710	1.204	0.7358	8.182	1.362	0.5734	2.005	1.246	0.5425	5.836	1.114	0.6899	0.97	1.24

[a] These parameters resulted from best-fit searches in analysis 1. The Coulomb potential is that of the deformed Fermi distribution where $r_c = 1.11$ fm and $a_c = 0.58$ fm and its multipole moments are set to equal to the WSFF multipole moments of the other parts.

[b] These parameters resulted from best-fit searches in analysis 2. The reduced radius and diffuseness parameters of the Coulomb potential are equal to those used in analysis 1 and its multipole moments are set to equal to the WSFF multipole moments of the spin-orbit part.

[c] χ^2 per data point for the elastic scattering.

This moment is introduced in order to compare the multipole moment of the imaginary part of the phenomenological DOP with that of the microscopic optical potential described in Sec. IV. The uncertainties in the multipole moments have been defined by the values where the χ^2 value increases by 5% from the minimum keeping the DOP parameters of the other parts fixed. In Figs. 4(a) and (b), we show the χ^2 contours as a function of the WSFF multipole moments of the real central and spin-orbit parts obtained by analysis 2. These figures show that the uncertainties of the multipole moments of the spin-orbit part are much larger than those of the real central part, but there is little correlation between the multipole moments of the real central and spin-orbit parts. Also the WSFF multipole moments of the volume imaginary and surface imaginary parts are not correlated with those of the real central part. Therefore we can evaluate the uncertainties of the multipole moments of each part independently. We have obtained reliable values of the hexadecapole moments because of the excellent fits for the 6^+ states.

The multipole moments of the real central part derived from analysis 2 are shown in Fig. 5 together with the results of the Er and Yb isotopes which have been obtained by our previous work.[10] As shown in Figs. 3 and 5, the quadrupole (Q_2) moment of each part decreases as the target mass number increases. This trend agrees with the well-known systematic behavior of the Y_{20} deformation of nucleus which has been already pointed out by the Nilsson model calculation[36] and also by the $B(E2)$ measurement. The hexadecapole (Q_4) moment decreases to a large negative value as the target mass number increases.

IV. DISCUSSION

A. Quadrupole moment

The multipole moments obtained by other experiments are also presented in Table IV together with our results. The charge Q_2 moments from Ronningen *et al.*[20] and from Lee *et al.*[21] using Coulomb excitation are plotted in Fig. 3. The most striking feature of these results is that the Q_2 moment of the real central part in the present work is 6–9% larger than the charge Q_2 moment obtained by Coulomb excitation for all the measured nuclei. According to our previous work,[10] this difference is mainly attributed to the density dependence of the effective interaction. The results of the folding model calculation using a realistic effective interaction will be described in Sec. IV C. For the W isotopes, the Q_2 moment of the real central part from our study is in good agreement with that from the 24 MeV (α,α') data of Baker *et al.*[16]

As shown in Fig. 3 and Table IV, the WSFF Q_2 moment of the spin-orbit part is smaller than that of the real central part and agrees with the charge Q_2 moment within the fitting error for all the measured nuclei. This trend is in accordance with that of the microscopic optical potential,[37] where the effect of the density dependence on the spin-orbit part for the spin-saturated nuclei is very small.

The potential Q_2 moment of the imaginary part is not so different from the charge Q_2 moment for all the mea-

TABLE III. Deformation parameters of best fit DOP of analysis 1 and analysis 2.

	β_2^R	β_4^R	β_6^R	β_2^{wv}	β_4^{wv}	β_6^{wv}	β_2^{ws}	β_4^{ws}	β_6^{ws}
Nucleus	β_2^{ls}	β_4^{ls}	β_6^{ls}	β_2^{c}	β_4^{c}	β_6^{c}	$\chi^2/N(2^+)$	$\chi^2/N(4^+)$	$\chi^2/N(6^+)$
^{178}Hf[a]	0.2470	−0.0438	−0.0058	0.2924	−0.0558	−0.0071	0.2462	−0.0448	−0.0068
	0.2770	−0.0538	−0.0086	0.3036	−0.0640	−0.0128	1.82	3.63	12.24
^{180}Hf[a]	0.2431	−0.0567	−0.0020	0.3039	−0.0792	−0.0024	0.2366	−0.0558	−0.0025
	0.2836	−0.0738	−0.0032	0.3001	−0.0843	−0.0056	1.74	4.21	15.19
^{182}W[a]	0.2256	−0.0566	0.0014	0.3641	−0.0122	0.0060	0.2349	−0.0616	0.0014
	0.2602	−0.0720	0.0019	0.2822	−0.0859	0.0015	1.92	3.04	35.47
^{184}W[a]	0.2183	−0.0622	0.0037	0.2817	−0.0927	0.0066	0.2153	−0.0621	0.0036
	0.2535	−0.0804	0.0052	0.2700	−0.0938	0.0057	1.86	2.56	27.62
^{178}Hf[b]	0.2529	−0.0401	−0.0160	0.2045	−0.1017	0.0827	0.2724	0.0163	−0.1704
	0.2572	−0.0484	0.0230	0.2719	−0.0579	0.0306	1.10	2.81	0.89
^{180}Hf[b]	0.2507	−0.0562	−0.0110	0.1965	−0.0983	0.0812	0.2514	0.0145	−0.2159
	0.2613	−0.0575	0.0354	0.2754	−0.0699	0.0479	1.28	3.47	1.12
^{182}W[b]	0.2382	−0.0579	−0.0107	0.1805	−0.0956	0.0926	0.2238	0.0090	−0.2440
	0.2458	−0.0654	0.0250	0.2574	−0.0771	0.0330	1.45	2.00	1.65
^{184}W[b]	0.2253	−0.0615	−0.0027	0.1761	−0.1132	0.0970	0.2403	−0.0773	−0.2640
	0.2390	−0.0812	0.0263	0.2462	−0.0934	0.0340	1.68	1.69	1.80

[a] Deformation parameters obtained by analysis 1.
[b] Deformation parameters obtained by analysis 2.

sured nuclei. However, according to the prediction of Brieva and Georgiev,[38] the imaginary part peaks out from the nuclear center in the low energy region and the Q_2 moment of the imaginary part is about 12% larger than that of the charge density at 65 MeV for ^{154}Sm. They also predicted that this difference became smaller with the increase of the incident energy and tended to zero for $E > 150$ MeV. Our results at 65 MeV do not agree with their prediction. With respect to the imaginary part, since the microscopic theory of the optical potential is still in a primitive stage, we do not make a detailed comparison between our phenomenological optical potential and the microscopic one at present.

B. Hexadecapole moment

As shown in Fig. 5, the Q_4 moments of the real central part for the Hf and W isotopes are connected smoothly with those for the Er and Yb isotopes and they decrease to large negative values as the target mass number increases.

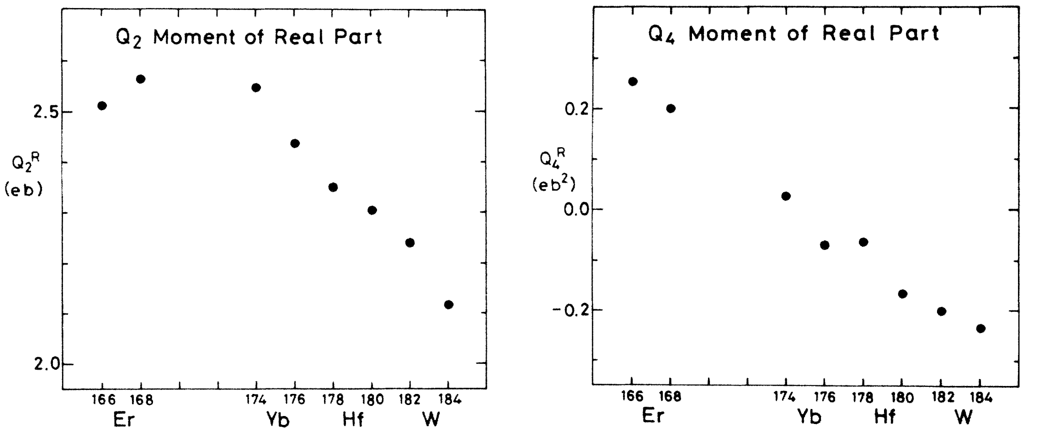

FIG. 5. The WSFF multipole moments of the real central part obtained by the coupled channel analysis. Those of the Er and Yb isotopes are the results of our previous work (Ref. 10). Those of the Hf and W isotopes are the results of analysis 2.

TABLE IV. Multipole moments of the DOP obtained in this work together with other results.

Nucleus	Reaction	Real (or charge)		Imaginary (potential)		Spin orbit (WSFF)		References
		$Q_2(eb)$	$Q_4(eb^2)$	$Q_2(eb)$	$Q_4(eb^2)$	$Q_2(eb)$	$Q_4(eb^2)$	
^{178}Hf	(p,p′) 65 MeV	2.311(22)	−0.083(13)					analysis 1
	(p,p′) 65 MeV	2.350(24)	−0.065(12)	2.286(118)	−0.415(79)	2.081(92)	−0.030(30)	analysis 2
	Coulomb excitation	2.204(12)	$0.23(^{15}_{21})$ −0.67(20)					20
	folded	2.103	−0.043	2.478	−0.057			a
^{180}Hf	(p,p′) 65 MeV	2.260(24)	−0.174(13)					analysis 1
	(p,p′) 65 MeV	2.304(35)	−0.170(14)	2.175(139)	−0.455(98)	2.098(107)	−0.059(36)	analysis 2
	Coulomb excitation	2.176(10)	$0.21(^{11}_{16})$ −0.65(16)					20
	folded	2.122	−0.074	2.507	−0.113			a
^{182}W	(p,p′) 65 MeV	2.182(24)	−0.201(13)					analysis 1
	(p,p′) 65 MeV	2.231(24)	−0.205(11)	2.073(133)	−0.465(87)	2.006(90)	−0.141(29)	analysis 2
	Coulomb excitation	2.053(15)	$-0.63(^{34}_{16})$					21
	(α,α') 13–21 MeV	2.053	−0.30					21
	(α,α') 24 MeV	2.13(10)	−0.775(196)					16
	(p,p′) 134 MeV	2.03(6)	$-0.25(^{13}_{33})$					11
	folded	2.028	−0.161	2.420	−0.222			a
^{184}W	(p,p′) 65 MeV	2.080(27)	−0.249(12)					analysis 1
	(p,p′) 65 MeV	2.117(25)	−0.238(11)	2.068(132)	−0.509(94)	1.896(120)	−0.232(32)	analysis 2
	Coulomb excitation	1.94(2)	−0.68(25)					21
	(α,α') 12.5–19 MeV	1.94	−0.243					21
	(α,α') 24 MeV	2.30(21)	−0.427(122)					16
	folded	1.919	−0.258	2.314	−0.358			a

[a] These are the results of the folding model calculation in this work.

This trend is also in accordance with that of the Y_{40} deformation obtained by (α,α') experiments at 50 MeV.[14] For the systematic behavior of the Q_4 moment of nuclei with $A=152-190$, a simple explanation has been given.[39] The Q_λ moments are proportional to the integral $\int_{\mu_0}^{1} P_\lambda(\mu)d\mu$ where $P_\lambda(\mu)$ is the λth Legendre polynomial, and $\mu_0=\cos\theta_0$ where θ_0 is the polar angle from the symmetry axis. At the beginning of the shell, added nucleons are placed in orbits as close to the symmetry axis as possible for prolate orbitals. Eventually, the equatorial orbits are again filled to make a spherically symmetric distribution with shell closure. The quantity μ_0 thus varies from 1 to 0 as more and more nucleons are added.

For the Hf isotopes, Ronningen *et al.*[20] have presented two different values of the charge Q_4 moment, one is positive and the other is negative. Our values of the real central part are negative, but our results are much smaller in magnitude than the negative values of the charge Q_4 moment. Also for the W isotopes, our results of the real central part are much smaller in magnitude than the charge Q_4 moments from Coulomb excitation by Lee *et al.*[21] The Q_4 moments of the real central part in the present work do not agree well with the values from the 24 MeV (α,α') data[16] for the W isotopes. As pointed out by some authors,[6,26] the discrepancy between multipole moments from (α,α') scattering and those from (p,p′) scattering could be an indication that α-particle scattering potentials are not derivable from the folding model.

As shown in Fig. 3 and Table IV, the Q_4 moment of the real central part is slightly smaller than the WSFF Q_4 moment of the spin-orbit part for all the measured nuclei. This trend is explainable considering that the effect of the density dependence on the spin-orbit part of the microscopic optical potential[37] is very small as mentioned above. The potential Q_4 moment of the imaginary part is more negative than the Q_4 moment of the real central part for all the measured nuclei and it decreases to a large negative value as the target mass number increases.

C. Folding model calculation

In the previous sections, we have discussed the multipole moment of the individual parts of the DOP obtained by the coupled channel analysis. In this section, we report on the results of a folding model calculation for the real central and imaginary parts using a realistic effective interaction and assuming a reasonable matter distribution.

According to Brieva and Rook,[40] the folded potential is expressed as

$$\begin{aligned} U_{\rm p}(\mathbf{r}_1,E)=&\int \rho_{\rm p}(\mathbf{r}_2)T_D^{\rm pp}(\,|\mathbf{r}_1-\mathbf{r}_2|\,;\rho(\mathbf{R}),E)d\mathbf{r}_2+\int \rho_{\rm n}(\mathbf{r}_2)T_D^{\rm pn}(\,|\mathbf{r}_1-\mathbf{r}_2|\,;\rho(\mathbf{R}),E)d\mathbf{r}_2\\ &+\int \rho_{\rm p}(\mathbf{r}_1,\mathbf{r}_2)T_{\rm ex}^{\rm pp}(\,|\mathbf{r}_1-\mathbf{r}_2|\,;\rho(\mathbf{R}),E)j_0(k\,|\mathbf{r}_1-\mathbf{r}_2|\,)d\mathbf{r}_2\\ &+\int \rho_{\rm n}(\mathbf{r}_1,\mathbf{r}_2)T_{\rm ex}^{\rm pn}(\,|\mathbf{r}_1-\mathbf{r}_2|\,;\rho(\mathbf{R}),E)j_0(k\,|\mathbf{r}_1-\mathbf{r}_2|\,)d\mathbf{r}_2\ , \end{aligned} \tag{9}$$

with

$$\rho_{\rm p,n}(\mathbf{r}_1,\mathbf{r}_2)=\rho_{\rm p,n}(\mathbf{R})\frac{3}{s^3k_F^3}[\sin(sk_F)-(sk_F)\cos(sk_F)]\ , \tag{10}$$

where $s=|\mathbf{r}_1-\mathbf{r}_2|$, $\mathbf{R}=(\mathbf{r}_1+\mathbf{r}_2)/2$, $j_0(x)$ is a Bessel function of order zero, and $\rho_{\rm p}$ and $\rho_{\rm n}$ represent the proton and neutron distributions, respectively. For the case of incident protons, the direct part $(T_D^{\rm pp},T_D^{\rm pn})$ and the exchange part $(T_{\rm ex}^{\rm pp},T_{\rm ex}^{\rm pn})$ of the effective interaction are given by

$$\begin{aligned} T_D^{\rm pp}&=(t^{01}+3t^{11})/4\ ,\\ T_{\rm ex}^{\rm pp}&=(t^{01}-3t^{11})/4\ ,\\ T_D^{\rm pn}&=(3t^{10}+t^{01}+t^{00}+3t)/8\ ,\\ T_{\rm ex}^{\rm pn}&=(3t^{10}+t^{01}-t^{00}-3t^{11})/8\ , \end{aligned} \tag{11}$$

where pp and pn stand for the proton-proton and proton-neutron interaction, respectively, and t^{ST} are the nucleon effective interactions and of the density-dependent effective interaction is that of complex effective potential with Gaussian form factor (CEG).[41] It parametrizes the effective interaction by a linear combination of Gaussian form factors with three ranges, and each coefficient is a function of Fermi momentum k_F and of the energy of the projectile in nuclear matter $E(r)$. [$E(r)=E_{in}-V_{\rm Coul}(r)$, where $V_{\rm Coul}(r)$ represents the Coulomb potential.] The imaginary potential is derived from the product of the effective k mass[42–44] and the imaginary part of Eq. (9) as

$$W=\frac{m_k}{m}{\rm Im}[U_{\rm p}(\mathbf{r}_1,E)]\ , \tag{12}$$

where the effective k mass is expressed as

$$\frac{m_k}{m}=\left[1+\frac{\partial V_\infty}{\partial k}\right]^{-1}\ , \tag{13}$$

and its numerical values are calculated using the approximate relation by Jeukenne *et al.*[45]

In this calculation, the point nucleon matter distribution used was the deformed Fermi one. The matter diffuseness a_m was fixed as $a_m=0.47$ fm (Ref. 1) and the matter radius was determined according to the following relation:[46]

$$\langle r^2\rangle_{\rm p}=\langle r^2\rangle_{\rm charge}-0.76+0.11(N/Z)\ ({\rm fm}^2)\ , \tag{14}$$

where $\langle r^2\rangle_{\rm p}$ and $\langle r^2\rangle_{\rm charge}$ represent the mean square radii of the point proton distribution and the charge density, respectively. The density-dependent Hartree-Fock (DDHF) calculation by Negele and Rinker[47] showed that the multipole moments of the point proton and point neutron distributions are different for the neighboring rare earth nuclei, while the proton inelastic scattering from ^{154}Sm and ^{176}Yb at 800 MeV (Ref. 7) suggested that the multipole moments of the proton and neutron distributions were almost identical. Thus at present, the difference between the multipole moments of the proton and neutron distributions is not confirmed. Therefore we assumed that the multipole moments of the point proton distribution are equal to those of the point neutron distribution also for the Hf and W isotopes. In our previous folding model calculation for the Er and Yb isotopes,[10] we have used the multipole moments obtained by the Bates (e,e′) experiments[17,18] for those of the point nucleon matter distribution. However there are no such data for the Hf and W isotopes. Although the charge Q_2 moments obtained from Coulomb excitation[20,21] are available for all the measured nuclei, the charge Q_4 moments for the Hf isotopes by Ronningen *et al.*[20] have the sign-amplitude ambiguity. The two values for the W isotopes by Lee *et al.*[21] (one is from Coulomb excitation and the other is from Coulomb-nuclear interference data) are inconsistent with each other. Thus, at present, we do not use these data as the multipole moments of the point nucleon matter distribution. As discussed in Sec. IV A, the WSFF Q_2 moments of the spin-orbit part of the DOP obtained by the coupled channel analysis agree with those of the charge density obtained by the Coulomb excitation within the fitting errors. Therefore we substituted the WSFF multipole moments of the spin-orbit part of the DOP obtained by analysis 2 for those of the point nucleon matter distribution. The parameters of the point nucleon matter distributions used are listed in Table V.

The results of the folding calculation are listed in Table IV and also plotted in Fig. 3. The Q_2 moments of the real central part of the folded potential show an increase of about 1% over those of the point nucleon matter distribution, which were set to be equal to the WSFF Q_2 moments of the spin-orbit part obtained by analysis 2. But they are a little smaller than the results of analysis 2 for all the measured nuclei. According to the calculation by Brieva and Georgiev,[38] the Q_2 moment of the folded potential exhibits an increase of about 4% over that of the matter distribution for ^{154}Sm at 65 MeV. The rate of increase of the Q_2 moment mainly depends on the matter distribution and the effective interaction used in the folding model calculation. Since the effect of the different matter distributions is estimated to be about 0.5%, the main part of this difference between our result and theirs is attributed to the different effective interactions used. In Fig. 3 and Table IV, we notice that the Q_4 moments of the real folded potential agree well with those derived from analysis 2. By our experimental data at 65 MeV, we can determine the phenomenological DOP fairly well in the nuclear surface region, but this phenomenological DOP seems to contain some ambiguity in the inner region. Since the Q_4 moment is sensitive to the potential shape of the nuclear surface region, the Q_4 moment is not influenced so much by the ambiguity in the inner region of the DOP.

TABLE V. Matter distributions

	^{178}Hf	^{180}Hf	^{182}W	^{184}W
R_m (fm)	6.373	6.397	6.421	6.444
a_m (fm)	0.470	0.470	0.470	0.470
β_2^m	0.2722	0.2755	0.2575	0.2462
β_4^m	−0.0580	−0.0699	−0.0771	−0.0934
β_6^m	0.0306	0.0479	0.0331	0.0340
Q_2 $(eb)^a$	2.081	2.098	2.006	1.896
Q_4 $(eb^2)^a$	−0.030	−0.059	−0.141	−0.232
Q_6 $(eb^3)^a$	0.041	0.076	0.032	0.022

[a]These multipole moments are equal to the WSFF multipole moments of the spin-orbit part derived from analysis 2.

With respect to the imaginary part, the Q_2 moment of the folded potential is about 20% larger than that of the point nucleon matter distribution and exceeds the Q_2 moment of analysis 2 by 10–15 %. In this energy region, the Q_2 moment of the imaginary part is expected to be larger than that of the charge density owing to the surface term.[38] But our results from analysis 2 are not so much different from that of the charge density for all the measured nuclei. Also the Q_4 moment of the imaginary folded potential is considerably different from that derived from analysis 2. These differences may be attributed to some effects which are not sufficiently taken into account in the imaginary part of the microscopic optical potential.

V. SUMMARY AND CONCLUSIONS

We have measured the differential cross sections and the analyzing powers of elastic and inelastic scattering of 65 MeV polarized protons from ^{178}Hf, ^{180}Hf, ^{182}W, and ^{184}W. In the framework of the coupled channel formalism, we have analyzed these data for the members of the ground state rotational band up to the 6^+ state assuming the axially symmetric rotational model. In this analysis, all the deformation parameters of the real central, volume imaginary, surface imaginary, and spin-orbit parts of the DOP were searched independently and excellent fits have been obtained for the 0^+, 2^+, 4^+, and 6^+ states for all the measure nuclei.

The WSFF Q_2 moment of the real central and spin-orbit parts of the DOP and the potential Q_2 moment of the imaginary part of the DOP decreases as the target mass number increases. The Q_4 moment decreases to a large negative value as the target mass number increases. These trends are consistent with the systematic behaviors of the Y_{20} and Y_{40} deformation of "rare earth region nuclei" ($A = 152$–190) which have been already pointed out by both the experimental and theoretical investigation.[14,36,39]

The Q_2 moment of the real central part in the present study is 6–9 % larger than the charge Q_2 moment[20,21] for all the measured nuclei. On the other hand, the WSFF Q_2 moment of the spin-orbit part agrees with the charge Q_2 moment within the uncertainty of the fitting. These trends are consistent with the difference between the effects of the density dependence of the effective interaction on the real central part and the spin-orbit part of the optical potential. The potential Q_2 moment of the imaginary part is not so much different from the charge Q_2 moment. This result does not agree with the prediction by Brieva and Georgiev[38] that the Q_2 moment of the imaginary part is about 12% larger than that of the charge density owing to the surface term.

A folding model calculation using the realistic density dependent effective interaction (CEG) (Ref. 41) has been carried out. In this calculation, the point nucleon matter distribution was derived from the global fit[1,46] and its multipole moments used were chosen so as to reproduce the same values of the WSFF multipole moments of the spin-orbit part derived from the coupled channel analysis. As for the real central part, the Q_2 moment of the folded potential is a little smaller than that derived from the coupled channel analysis, while the Q_4 moment is well reproduced by the folded potential. With respect to the imaginary part, the folding model did not reproduce either the Q_2 moment or the Q_4 moment derived from the coupled channel analysis. Further progress in the microscopic treatment of the imaginary part of the optical potential is necessary.

Finally, the excellent fits to the cross sections and the analyzing powers of ground band rotational states up to 6^+ excited by 65 MeV polarized protons indicate that the relation of the multipole moments of the same order among each part of the DOP is not so simple as described by the same deformation parameter, or the same deformation length (βR), or the same multipole moment. The multipole moments of the individual parts of the DOP reflect the characteristics of the corresponding components of the effective nucleon-nucleon interaction and it is found that they are useful in examining various microscopic optical potentials.

ACKNOWLEDGMENTS

The authors wish to express their thanks to Professor H. Ikegami, Professor S. Morinobu, Dr. M. Fujiwara, and Dr. Y. Fujita for their advice in the operation of the spectrograph RAIDEN and its focal counter system and to Dr. K. Hatanaka for the operation of the polarized ion source. We are indebted to Dr. Sugai at the Institute for Nuclear Study, University of Tokyo for his advice and cooperation in target preparation. Sincere thanks are also expressed to Professor S. Nagata at Miyazaki University for the usage of his effective interaction and for his advice and discussion in calculating the folded potentials. One of the authors (H.O.) is grateful to Professor N. Shiomi and Professor N. Sakamoto at Nara Women's University for their encouragement. The coupled channel analysis and the folding model calculation were done with FACOM M-180-2AD at RCNP, FACOM M-382 at Data Processing Center, Kyoto University, and FACOM M-340 at the Department of Physics, Kyoto University. The experiment has been performed at the Research Center for Nuclear Physics, Osaka University under Program Nos. 15A18 and 16A21 and was supported in part by a Grant-in-Aid for Scientific Research No. 58460016 of the Japan Ministry of Education, Science and Culture.

---

[*] Present address: Nara Women's University, Nara 630, Japan.

[†] Present address: Research Center for Nuclear Physics, Osaka 567, Japan.

[‡] Present address: Institute of Physics, University of Tsukuba, Niihari-Gun, Ibaraki 305, Japan.

[§] Present address: Institute of Physical and Chemical Research, Wako, Saitama 351, Japan.

[**] Present address: Sanyo Electric Co., Ltd., Osaka 573, Japan.

[1] H. Sakaguchi, M. Nakamura, K. Hatanaka, A. Goto, T. Noro, F. Ohtani, H. Sakamoto, H. Ogawa, and S. Kobayashi, Phys. Rev. C **26**, 944 (1982).

[2] P. Schwandt, H. O. Meyer, W. W. Jacobs, A. D. Bacher, S. E. Vigdor, and M. D. Kaitchuck, Phys. Rev. C **26**, 55 (1982).

[3] A. Nadasen, P. Schwandt, P. P. Singh, W. W. Jacobs, A. D. Bacher, P. T. Debevec, M. D. Kaitchuck, and J. T. Meek, Phys. Rev. C **23**, 1023 (1981).

[4] E. Fabrici, S. Micheletti, M. Pignanelli, F. G. Resmini, R. DeLeo, G. D'Erasmo, A. Pantaleo, J. L. Escudie, and A. Tarrats, Phys. Rev. C **21**, 830 (1980).

[5] E. Fabrici, S. Micheletti, M. Pignanelli, F. G. Resmini, R. DeLeo, G. D'Erasmo, and A. Pantaleo, Phys. Rev. C **21**, 844 (1980).

[6] C. H. King, J. E. Finck, G. M. Crawley, J. A. Nolen, Jr., and R. M. Ronningen, Phys. Rev. C **20**, 2084 (1979).

[7] M. L. Barlett, J. A. McGill, L. Ray, M. M. Barlett, G. W. Hoffman, N. M. Hintz, G. S. Kyle, M. A. Franey, and G. Blanpied, Phys. Rev. C **22**, 1168 (1980).

[8] R. M. Ronningen, G. M. Crawley, N. Anantaraman, S. M. Banks, B. M. Spicer, G. G. Shute, V. C. Officer, J. M. R. Wastell, D. W. Devins, and D. L. Friesel, Phys. Rev. C **28**, 123 (1983).

[9] F. Ohtani, H. Sakaguchi, M. Nakamura, T. Noro, H. Sakamoto, H. Ogawa, T. Ichihara, M. Yosoi, and S. Kobayashi, Phys. Rev. C **28**, 120 (1983).

[10] T. Ichihara, H. Sakaguchi, M. Nakamura, T. Noro, F. Ohtani, H. Sakamoto, H. Ogawa, M. Yosoi, M. Ieiri, N. Isshiki, and S. Kobayashi, Phys. Rev. C **29**, 1228 (1984).

[11] B. G. Lay, S. M. Banks, B. M. Spicer, G. G. Shute, V. C. Officer, R. M. Ronningen, G. M. Crawley, N. Anantaraman, and R. P. DeVito, Phys. Rev. C **32**, 440 (1985). This paper appeared concurrently with the submission of our paper. Their value of the Q_2 moment is about 7% smaller than our result and almost equal to the charge Q_2 moment. Considering the effect of the density dependence of the effective interaction at their energy (Ref. 38), their value seems to be a little small. The Q_4 moments of our study and theirs are in good agreement.

[12] H. Clement, R. Frick, G. Graw, F. Merz, H. J. Scheerer, P. Schiemenz, N. Seichert, and S. T. Hsun, Phys. Rev. Lett. **48**, 1082 (1982).

[13] K. Hatanaka, N. Matsuoka, T. Saito, K. Hosono, M. Kondo, S. Kato, T. Higo, S. Matsuki, and K. Ogino, Nucl. Phys. **A403**, 109 (1983).

[14] D. L. Hendrie, N. K. Glendenning, B. G. Harvey, O. N. Javis, H. H. Duhm, J. Saudinos, and J. Mahoney, Phys. Lett. **26B**, 127 (1968).

[15] N. K. Glendenning, D. L. Hendrie, and O. N. Javis, Phys. Lett. **26B**, 130 (1968).

[16] F. T. Baker, A. Scott, R. C. Styles, T. H. Kruse, K. Jones, and R. Suchannek, Nucl. Phys. **A351**, 63 (1981).

[17] T. Cooper, W. Bertozzi, J. Heisenberg, S. Kowalski, W. Turchinetz, C. Williamson, L. Cardman, S. Fivozinsky, J. Lightbody, Jr., and S. Penner, Phys. Rev. C **13**, 1083 (1976).

[18] C. W. Creswell, Ph.D. thesis, MIT, 1977 (unpublished).

[19] T. Sasamura, Ph.D. thesis, MIT, 1979 (unpublished).

[20] R. M. Ronningen, J. H. Hamilton, L. Varnell, J. Lange, A. V. Ramayya, G. Garcia-Bermudez, W. Lourens, L. L. Riedinger, F. K. McGowan, P. H. Stelson, R. L. Robinson, and J. L. C. Ford, Jr., Phys. Rev. C **16**, 2208 (1977).

[21] I. Y. Lee, J. X. Saladin, J. Holden, J. O'Brien, C. Baktash, C. E. Bemis, Jr., P. H. Stelson, F. K. McGowan, W. T. Milner, J. L. Ford, Jr., R. L. Robinson, and W. Tuttle, Phys. Rev. C **12**, 1483 (1975).

[22] R. M. Ronningen, F. Todd Baker, Alan Scott, T. H. Kruse, R. Suchannek, W. Savin, and J. H. Hamilton, Phys. Rev. Lett. **40**, 364 (1978).

[23] H. Fisher, D. Kamke, H. J. Kittling, E. Kuhlmann, H. Plicht, and R. Schormann, Phys. Rev. C **15**, 921 (1977).

[24] K. A. Erb, J. E. Holden, I. Y. Lee, J. X. Saladin, and T. K. Saylor, Phys. Rev. Lett. **29**, 1010 (1972).

[25] G. R. Satchler, J. Math. Phys. **13**, 1118 (1972).

[26] R. S. Mackintosh, Nucl. Phys. **A266**, 379 (1976).

[27] H. Ikegami, S. Morinobu, I. Katayama, M. Fujiwara, and S. Yamabe, Nucl. Instrum. Methods **175**, 335 (1980).

[28] K. Imai, N. Tamura, and K. Nishimura, Research Center for Nuclear Physics Annual Report, 1976, p. 76.

[29] T. Ichihara, H. Sakaguchi, K. Hatanaka, M. Fujiwara, and K. Hosono, Research Center for Nuclear Physics Annual Report, 1981, p. 194.

[30] G. Sletten and P. Knudsen, Nucl. Instrum. Methods **102**, 459 (1972).

[31] Y. Fujita, K. Nagayama, M. Fujiwara, S. Morinobu, T. Yamazaki, and H. Ikegami, Nucl. Instrum. Methods **196**, 249 (1982).

[32] I. Katayama and H. Ogata, Nucl. Instrum. Methods **174**, 295 (1980).

[33] S. Morinobu, private communications.

[34] J. Raynal, code ECIS79, Saclay (unpublished).

[35] J. Raynal, International Atomic Agency Report IAEA-5MR-818, 1972, p. 75.

[36] B. R. Mottelson and S. G. Nilsson, K. Dans. Vidensk. Selsk. Mat.-Fys. Skr. **1**, No. 8 (1959).

[37] F. A. Brieva and J. R. Rook, Nucl. Phys. **A297**, 206 (1978).

[38] F. A. Brieva and B. Z. Georgiev, Nucl. Phys. **A308**, 27 (1978).

[39] G. F. Bertsch, Phys. Lett. **26B**, 130 (1968); M. A. Preston and R. K. Bhaduri, *Structure of the Nucleus* (Addison-Wesley, Reading, Mass., 1975).

[40] F. A. Brieva, and J. R. Rook, Nucl. Phys. **A291**, 317 (1977).

[41] N. Yamaguchi, S. Nagata, and T. Matsuda, Prog. Theor. Phys. **73**, 459 (1983); and private communications.

[42] V. Bernard and Nguyen Van Giai, Nucl. Phys. **A327**, 397 (1979).

[43] S. Fantoni, B. L. Friman, and V. R. Pandharipande, Phys. Lett. **104B**, 89 (1981).

[44] J. W. Negele and K. Yazaki, Phys. Rev. Lett. **47**, 71 (1981).

[45] J. P. Jeukenne, A. Lejeune, and C. Mahaux, Phys. Rev. C **15**, 10 (1977).

[46] G. R. Satchler and W. G. Love, Phys. Rep. **55**, 183 (1979).

[47] J. W. Negele and G. Rinker, Phys. Rev. C **15**, 1499 (1977).